Near-Infrared Photoluminescence of Single-Walled Carbon Nanotubes Prepared by the Laser Vaporization Method

Sergei Lebedkin,*,† Frank Hennrich,† Tatyana Skipa,‡ and Manfred M. Kappes†,§

Institut für Nanotechnologie and Institut für Festkörperphysik, Forschungszentrum Karlsruhe, D-76021 Karlsruhe, Germany, and Institut für Physikalische Chemie, Universität Karlsruhe, D-76128 Karlsruhe, Germany

Received: September 29, 2002; In Final Form: December 23, 2002

Single-walled carbon nanotubes (SWNTs) prepared by pulsed laser vaporization, dispersed, and surfactant-stabilized in near-infrared transparent D_2O show weak photoluminescence (PL) from ~1300 up to >1750 nm corresponding to the lowest electronic interband transitions of semiconducting tubes. The characteristic features of this PL, such as a multiple peak emission and a strong excitation wavelength dependence (investigated for λ_{exc} from 457 up to 1064 nm), are similar to those reported recently for SWNTs with smaller diameters of around 1 nm (O'Connell et al. *Science* **2002**, *297*, 593). The luminescence is significantly polarized with an anisotropy value *r* of up to 0.32, depending on the excitation and emission wavelengths. The PL data can be used for the structural assignment of emitting tubes; however, in agreement with the results of O'Connell et al., these data are only qualitatively consistent with the tight-binding model widely applied for SWNTs. The luminescence is sensitive to chemical treatment/interactions of SWNTs; much weaker and broader PL was observed above 1300 nm for dispersions of acid-treated tubes in D_2O, whereas raw SWNTs in *N*,*N*-dimethylformamide show practically no PL. The Raman spectra of dispersed SWNTs differ from those of the solid samples.

1. Introduction

Optical properties of single-walled carbon nanotubes (SWNTs) have attracted substantial interest, regarding both the characterization of these materials[1,2] and possible practical applications, for instance, for optical limiting.[3] There have been a few reports of broad *visible* photoluminescence (PL) from chemically functionalized SWNTs in solution and SWNTs in polymeric matrixes[4,5] as well as from small-diameter nanotubes grown in zeolite channels.[6] The origin of this PL remains unclear, but for the treated nanotubes, it is perhaps caused by the structural defects and/or chemical groups attached to SWNTs.

Recently, O'Connell et al.[7] have discovered a relatively bright structured near-infrared (NIR) photoluminescence between ~900 and ~1400 nm from raw SWNTs ultrasonically dispersed in a D_2O−surfactant mixture. (The use of D_2O as a solvent instead of H_2O allows near-infared optical measurements with standard cuvettes up to ~1800 nm compared to ~1300 nm for H_2O.) These SWNTs were prepared by a high-pressure catalytic CO decomposition (the HiPco method) and have diameters between ~0.7 and ~1.1 nm.[8] PL measurements presumably correspond to individual nanotubes isolated and stabilized in surfactant micelles, following ultracentrifugation to separate individual tubes from bundles. In nanotube bundles, for instance, in solid samples, this PL appears to be strongly quenched via intertube interactions. The NIR luminescence emission and excitation bands correspond to the lowest interband transitions E_{11}^S and E_{22}^S between van Hove singularities (vHs) in the electronic density of states of semiconducting nanotubes[9] (Figure 1) and allow a direct measurement of the E_{11}^S and E_{22}^S energies.[7]

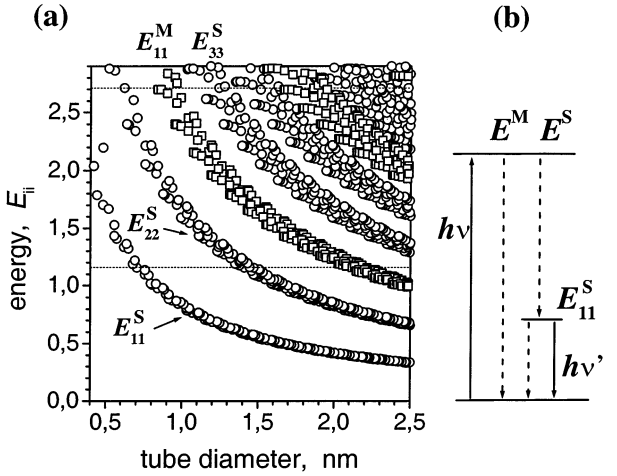

Figure 1. (a) Energy separations E_{ii} between van Hove singularities in semiconducting (circles) and metallic (squares) SWNTs as a function of diameter, *d*, calculated in the tight-binding model with $\gamma_0 = 2.9$ eV (ref 9). The four lowest branches E_{11}^S, E_{22}^S, E_{11}^M, and E_{33}^S relate to the S1, S2, M1, and S3 bands in the absorption spectra of SWNTs, respectively (Figure 2). The scatter of the energy values along the $E-d$ curves is due to the effect of trigonal warping on the energy dispersion relations (ref 17). The dashed lines denote the luminescence excitation range (1.16−2.71 eV) covered in this work. (b) Schematic plot of the optical excitation ($h\nu$) and electronic relaxation processes in SWNTs, where electronic relaxation in semiconducting nanotubes proceeds first to the lowest π^*-subband corresponding to the first van Hove singularity in density of states. Radiative relaxation from this state gives rise to the near-infrared luminescence ($h\nu'$).

Although the HiPco method is advantageous for a bulk production of carbon nanotubes, the majority of studies on

* Corresponding author. Fax: +49−7247−826368. E-mail: lebedkin@int.fzk.de.
† Institut für Nanotechnologie.
‡ Institut für Festkörperphysik.
§ Institut für Physikalische Chemie.

10.1021/jp027096z CCC: $25.00
Published on Web 02/08/2003

carbon nanotubes has so far been performed with SWNT materials obtained by other methods, in particular by the pulsed laser vaporization (PLV) of carbon targets containing a Ni/Co catalyst in an inert atmosphere.[10] This method provides defect-free SWNTs with a narrow diameter distribution between ~1.2 and ~1.4 nm. Because of the relatively high material quality and extensive characterization, these SWNTs are often termed "standard" nanotubes. Even in this narrow diameter range, there are expected to be about 10 metallic and 20 semiconducting tubes of different size and chirality that have different roll-up indices (*n*,*m*) (Figure 1).[9] An observation of the intrinsic NIR luminescence from these nanotubes not only would be interesting in itself, but could also facilitate an assignment of their structures/relative abundance which is still poorly known for the bulk material.

In this work, we found that D_2O−surfactant dispersions of carbon nanotubes prepared by the PLV method indeed show structured photoluminescence from ~1300 to >1750 nm (germanium detector limit), although much weaker than that reported for nanotubes with the smaller diameters.[7] We present luminescence spectra excited at laser wavelengths between 457 and 1064 nm, as well as luminescence anisotropy spectra. The experimental data are compared with tight-binding model calculations and with empirical E_{11}^S, $E_{22}^S - (n,m)$ assignment relations derived very recently by Bachilo et al. from the luminescence and Raman data for the HiPco nanotubes.[11]

2. Experimental Section

2.1. Materials and Treatments. SWNTs were produced by the PLV method as described in detail elsewhere.[12,13] According to electron microscopy and Raman and optical spectroscopy, the material produced contains up to ~50 wt % of SWNTs, with a narrow diameter distribution peaked at ~1.3 nm. It is very similar to SWNT materials obtained by this method in other groups[2,10] and characterized by numerous techniques.[9] Similar to the procedure of O'Connell et al.,[7] a small amount of as-prepared SWNTs was added to 1 mL of D_2O (Aldrich) containing 0.1−0.3 mg/mL of the Tween-80 nonionic surfactant (Roth, Germany) and dispersed with an ultrasonic tip for 10 min at ~100 W/cm^2 power. A dispersion was then centrifuged in a standard lab microcentrifuge for 1 h at 20000*g*. Subsequently, a supernatant solution (of neutral pH) was collected and used for luminescence measurements. A typical final concentration of nanotubes was estimated to be about 20 μg/mL. No signs of their aggregation and precipitation were observed over weeks.

Prolonged sonication in air (~1 h) was found to result in a decrease of the near-infrared PL of nanotubes and an increase of a weak "background" PL below ~1000 nm, likely due to sonochemical oxidation of nanotubes. Some part of the background PL might be due to fullerenes (~2 wt % in the raw SWNT material) and other organic impurities.

SWNTs dispersed in D_2O containing 5 mg/mL of sodium dodecyl sulfate cationic surfactant (SDS, also purchased from Roth) showed a similar structured near-infrared PL as the dispersions in D_2O/Tween-80. The latter surfactant was preferred to SDS[7] because of the very low "working" concentration (critical micelle concentration (CMC) ≈ 13 μg/mL compared to 2.4 mg/mL for SDS) and, consequently, a negligible NIR absorption. Note also that SDS is difficult to completely wash out of filtered SWNTs (so-called buckypapers).[13] A weak and broad near-infrared PL was observed for SWNT dispersions stabilized with 1 mg/mL of Triton X-100 (nonionic surfactant, CMC ≈ 0.18 mg/mL). The reason for the "quenching" of the PL in this suspension is not clear at the moment. Triton X-100 was rejected also, because of its strong visible PL tailing into the near-infrared, probably caused by impurities.

2.2. Spectroscopic Measurements. UV−visible−NIR absorption spectra were recorded on a Varian Cary 500 spectrophotometer. NIR photoluminescence was measured in the range of ~900−1750 nm with 10 nm spectral slits on a Spex Fluorolog-3 spectrometer equipped with a double-grating NIR emission monochromator and a liquid nitrogen cooled germanium detector (Edinburgh Instruments). Luminescence in the range of ~600−1100 nm was checked using a Hamamatsu R5108 photomultiplier. The NIR luminescence was relatively weak; therefore, lasers were applied for continuous wave excitation of samples at different wavelengths from 457 nm up to 1064 nm comprising a Spectra Physics BeamLock 2060 Ar-ion laser, 375B dye laser, 3900S Ti−sapphire laser, and a diode-pumped Nd:YAG laser. Typical laser power and fluence (unfocused) was 50−200 mW and 0.5−10 W/cm^2. Emission spectra were corrected for the wavelength-dependent instrumental response of the spectrometer. The quantum efficiency of the luminescence of SWNTs, φ_{PL}, was estimated from a comparison with the phosphorescence of singlet oxygen $^1O_2$ in toluene (λ_{em} = 1275 nm, $\varphi_{phos} = 4.3 \times 10^{-6}$)[14] photosensitized by fullerene C_{70} (prepared in this lab) with a quantum yield $\varphi(^1O_2) \approx 1$.[15] The measurements were performed at room temperature, using standard 4 mm quartz cuvettes in a 90°-geometry. As one can expect for carbon nanotubes,[3,9] dispersed SWNTs demonstrated an excellent long-time photostability under the intense laser irradiation.

Luminescence polarization measurements were performed using a Berek variable wave plate (New Focus) to rotate the laser polarization and a Glan−Thompson prism as an emission polarizer. The polarization factor $P(\lambda)$ is given for the general case by[16]

$$P(\lambda) = (I_{HH} I_{VV} - I_{HV} I_{VH})/(I_{HH} I_{VV} + I_{HV} I_{VH}) \qquad (1)$$

where I denotes luminescence spectra recorded with four different combinations of vertical (V) and horizontal (H) polarizations for both excitation (first letter) and emission (second letter). Polarization rotation of an excitation laser beam typically has a negligible effect on its position and intensity, as was the case in our experiments. One can easily show that $I_{HH} = I_{VH}$ in this case, and therefore, $P(\lambda)$ can be calculated from only two individual measurements by

$$P(\lambda) = (I_{VV} - I_{HV})/(I_{VV} + I_{HV}) \qquad (2)$$

Luminescence anisotropy, r, is related to P as $r = 2P/(3 - P)$. The maximal values of r for randomly oriented molecules are +0.4 and −0.2 for collinear and perpendicular absorption and emission transition moments, respectively.[16]

Raman spectra of solid SWNTs and their dispersions in D_2O/Tween-80 were obtained on a Jobin Yvon XY spectrometer using Ar-ion laser excitation lines and on a Bruker Equinox 55S/FRA106 FT-Raman spectrometer with Nd:YAG laser excitation at 1064 nm. Note that FT-Raman features of dispersed tubes were recorded simultaneously with their NIR luminescence. The corresponding spectrum (after instrumental response correction) agreed well with that measured conventionally, as described above.

Tight-binding model calculations were performed using the Mathematica software from Wolfram Research, following the procedure described in ref 17.

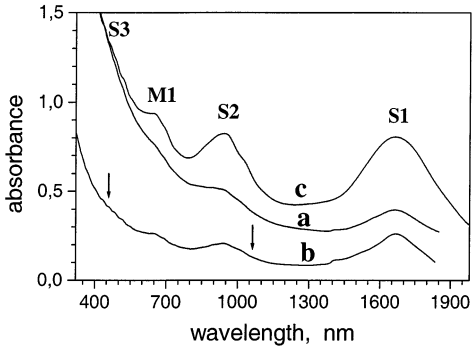

Figure 2. Optical absorption of SWNTs prepared by the laser vaporization and measured in a transmission mode: the raw material ultrasonically dispersed in D_2O/Tween-80 (a) before and (b) after centrifugation (10 mm cuvette, solvent absorption is subtracted) and (c) a free-standing ~300 nm thick film of SWNTs (ref 13). The arrows indicate the shortest (457 nm) and the longest (1064 nm) luminescence excitation wavelengths applied in this work.

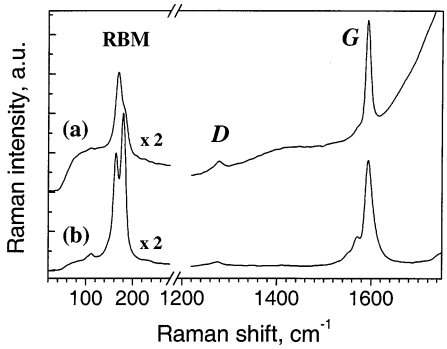

Figure 3. FT-Raman spectra of (a) SWNTs dispersed in D_2O/Tween-80 and (b) the raw SWNT material. The spectra are normalized to an equal intensity of the *G* band at 1594 cm^{-1} and offset for convenience. The strong background increase for dispersed nanotubes above ~1500 cm^{-1} is due to luminescence. Nd:YAG laser excitation at 1064 nm.

3. Results and Discussion

3.1. Preparation of SWNT Dispersions: Optical Absorption and Raman Spectra. The PLV carbon nanotubes, either dispersed/centrifuged in D_2O−Tween or prepared as a thin free-standing film,[13] show similar absorption bands S1, S2, S3 and M1 (Figure 2). In accordance with the tight-binding model, they have been attributed to optically allowed electronic transitions E_{11}^S, E_{22}^S, E_{33}^S, and E_{11}^M between pairs of vHs in the density of states of semiconducting and metallic nanotubes, respectively (Figure 1).[1,2,9] The broadening of the *S*1 band in the film is likely due to strong intertube interactions in SWNT bundles and agrees with theoretical predictions.[18] The major part of the background absorbance increasing strongly to the shorter wavelengths has been attributed to collective (π-plasmon) electronic excitations in nanotubes.[19] Attenuation of light transmitted through SWNT films and dispersions of the raw SWNT material (Figure 2a,c) is also, to some degree, due to light scattering.[20] One can expect that such dispersions contain, apart from finely distributed nanotubes, also large particles of amorphous carbon, metal catalysts, nanotube bundles, and/or aggregates thereof surrounded by surfactant molecules. Centrifugation efficiently removes such particles from the dispersion and results in much less light scattering (estimated visually), more pronounced absorption features of nanotubes (Figure 2b), and substantially increased NIR luminescence signals (see below).

Note that the absorption bands S1, S2, and M1 in Figure 2b are still rather structureless compared to the spectra reported for dispersed HiPco tubes. These presumably represent the absorption bands of individual, micelle-isolated nanotubes.[7] The broad absorption features suggest that our dispersions still contain many (small) nanotube aggregates/bundles. Indeed, we were able to centrifuge SWNT dispersions only at 20000*g* compared to 120000*g* applied by O'Connell et al.[7] Furthermore, one can expect that bundles of the PLV nanotubes have lower densities than bundles of the thinner HiPco nanotubes. Consequently, sedimentation upon centrifugation in D_2O will be much less effective.

On the other hand, the FT-Raman spectrum of the dispersed and centrifuged PLV tubes differs from that of the solid material (Figure 3). The former spectrum demonstrates a remarkably sharp *G*-band at 1594 cm^{-1}, with a strongly reduced lower frequency component at ~1570 cm^{-1}. The same trends were observed in the Raman spectra excited at 488 and 514.5 nm (not shown). It is interesting to note that a similar *G*-band shape has been observed for SWNTs functionalized with long-chain alkyl groups and dissolved—supposedly as individual tubes—in CS_2.[21] Compared to the solid, the relative intensity of the *D*-band at 1277 cm^{-1} is increased in dispersed nanotubes. The radial breathing modes pattern is also changed and somewhat downshifted compared to the solid samples; however, the change is less than the ~7% downshift predicted for isolated nanotubes.[22] The Raman results suggest different structural patterns/intertube interactions in SWNTs bundles in the solid state compared to a dispersion. The bundles are likely relatively small in the latter case. Raman features of dispersed carbon nanotubes deserve further investigation.

3.2. Luminescence Emission and Excitation Spectra. Figure 4 shows NIR luminescence spectra[23] of an SWNT dispersion in D_2O/Tween-80 measured under the same conditions at several laser excitation wavelengths between 457 and 1064 nm, covering the S2, M1, and partly S3 absorption bands of nanotubes (Figure 2). The complete set of emission spectra excited at 35 laser wavelengths is available as Supporting Information. Similar to the HiPco nanotubes,[7] the NIR luminescence of the PLV nanotubes corresponds to the *S*1 band in the absorption spectrum or, in other words, to the lowest vHs transitions E_{11}^S in semiconducting nanotubes (Figure 1). Similarly, the luminescence is structured and demonstrates a complex, resonance-like dependence on both the excitation and emission wavelengths. This is apparently due to the fact that many types of semiconducting nanotubes that have different emission energies E_{11}^S and PL excitation profiles (different E_{22}^S and E_{33}^S energies) are present in the suspension and contribute to the luminescence. The PL spectra become increasingly structureless in going to the longest emission wavelengths. This can be explained by the increasing number of different SWNTs per emission energy interval, as emission energy decreases. Emission energy varies roughly inversely with increasing nanotube diameter, *d* (Figure 1).

The PL spectra change dramatically upon scanning the excitation wavelength within the S2 and S3 absorption bands but remain practically constant when exciting between from 623 to 737 nm (Figure 4). The latter region corresponds to the M1 absorption of nonemitting metallic nanotubes. Optical excitations of semiconducting nanotubes in this region are off-resonance with vHs. Therefore, according to the tight-binding model calculation,[24] the corresponding oscillator strengths are relatively weak and roughly independent of the excitation energy. This is reflected in the constant PL spectra. In contrast, when the laser wavelength scans the S2 absorption band, different nanotubes with different vHs transition energies are excited, and their

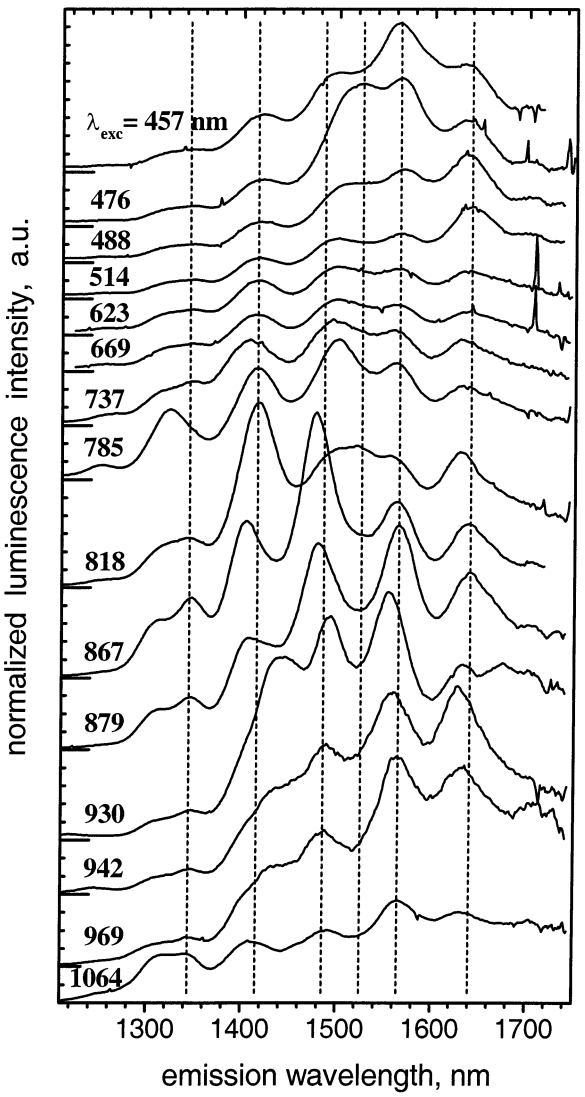

Figure 4. Near-infrared luminescence spectra of SWNTs in a D_2O/Tween-80 dispersion at selected laser excitation wavelengths. The spectra are normalized for the same excitation photon flux and offset vertically for clarity. The short horizontal lines denote zero intensity for each spectrum. The dotted vertical lines denote the emission wavelengths of the excitation profiles shown in Figure 5. The sharp peaks are due to muon spikes, they appear magnified above ~1650 nm, because the spectra are corrected for the wavelength-dependent spectrometer response.

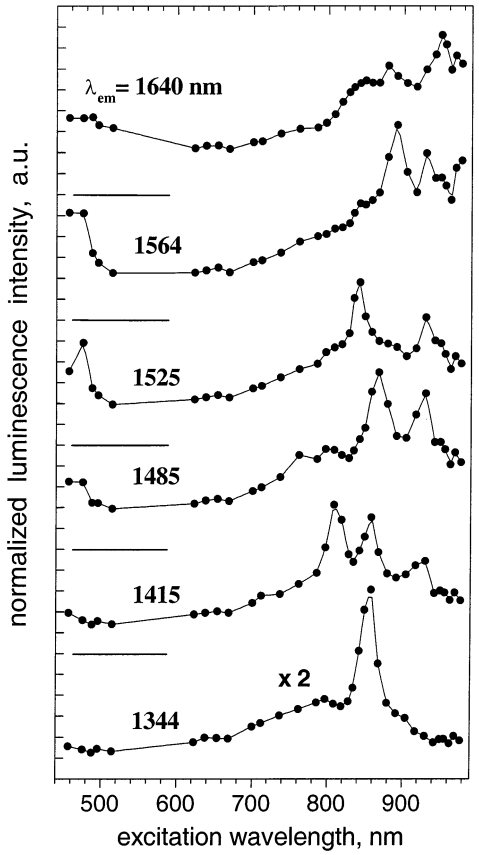

Figure 5. Luminescence excitation profiles for SWNTs dispersed in D_2O/Tween-80. They are obtained by slicing the whole set of luminescence spectra (see Supporting Information) over the indicated emission wavelengths. The profiles are vertically offset for clarity; the short horizontal lines denote zero intensities. The solid lines are interpolation curves drawn for convenience.

luminescence intensity demonstrates a resonance-like behavior similar to that of resonant Raman spectra of SWNTs.[9,22]

The excitation dependence of the PL is further illustrated by luminescence excitation profiles in Figure 5. The peaks in the range of $\lambda_{exc} \sim 800-1000$ nm correspond to the E_{22}^S optical excitations of specific semiconducting nanotubes and provide direct information about their E_{22}^S energies. There are only a few data points in the region of the S3 band (~400−530 nm); therefore, an estimation of the E_{33}^S energies was not attempted. Note that in contrast to the absorption spectrum (Figure 2b) the PL excitation profiles do not contain contributions from metallic nanotubes and plasmon excitations. As a result, the relative intensity of PL excited in the M1 region, i.e., between the S2 and S3 bands, is much lower than the corresponding relative absorption.

The most intense PL bands are observed to the blue (~1400−1600 nm) of the absorption maximum at 1667 nm (Figure 2). Their excitation resonances in the S2 band are similarly blue shifted relative to the S2 absorption maximum at 945 nm. In other words, nanotubes with diameters smaller than the mean value of ~1.3 nm corresponding to the S1 maximum are the most PL active. The most likely reason is a much higher quantum efficiency of the smaller semiconducting tubes. In fact, the PL spectra exhibit significant emission intensity at 1326 and 1346 nm, corresponding to ~1.1 nm nanotubes (Figure 4). These cannot be detected in the PLV material via optical absorption (Figure 2), Raman spectroscopy, or electron microscopy,[12,13] apparently because of their very low relative abundance (<1%). Of course, the surfactant or the centrifugation might in some way influence the diameter distribution of micelle-isolated (emitting) nanotubes relative to the raw material (see Experimental Section); however, this effect is not likely to be very significant.

Over the excitation wavelength range between 457 and 1064 nm, we find that the luminescence of dispersed PLV nanotubes is most efficient for *S*2 band excitation between ~820 and ~930 nm with an apparent total quantum yield of $\sim 7 \times 10^{-6}$ (the ratio of photons emitted between 1300 and 1750 nm to total photons absorbed). By taking into account that the emission extends beyond 1750 nm (Figure 4), one can estimate the total quantum yield as $\sim 1 \times 10^{-5}$. This is significantly less than the value of $\varphi_{PL} \sim 10^{-3}$ reported for HiPco nanotubes.[7] As discussed above, one reason for this difference may be that our dispersion still contained a high fraction of nonluminescent bundles. Another reason appears to be a general decrease of the efficiency of PL with increasing nanotube diameter. In any case, $\varphi_{PL} \sim 1 \times 10^{-5}$ is the average value over all absorbers

TABLE 1. Energies E_{11}^S and E_{22}^S of SWNTs Obtained from the Photoluminescence Spectra and Their (*n*,*m*) Assignment Based on the Empirical Relations of Bachilo et al. (Ref 11, Energy Values in Parentheses Were Calculated Using the C−C Bond Length of 0.144 nm)[a]

E_{11}^S, eV expt (calcd)	E_{22}^S, eV expt (calcd)	(*n*,*m*)	*d*, nm	α, grad
0.756 (0.754)	1.412 (1.411)	(13,6)	1.335	18.0
0.759 (0.759)	∼1.26[b] (1.236)	(14,6)	1.411	17.0
0.761 (0.766)	1.308 (1.304)	(11,9)	1,377	26.7
0.792 (0.794)	1.395 (1.389)	(10,9)	1.307	28.3
0.793 (0.796)	∼1.26[b] (1.242)	(16,2)	1.357	5.8
0.798 (0.802)	1.340 (1.322)	(12,7)	1.321	21.4
0.813 (0.811)	1.473 (1.475)	(11,7)	1.248	22.7
0.826 (0.822)	1.548 (1.556)	(12,5)	1.201	16.6
0.832 (0.834)	1.340 (1.330)	(13,5)	1.278	15.6
0.839 (0.843)	1.440 (1.419)	(10,8)	1.240	26.3
0.860 (0.871)	1.340 (1.330)	(15,1)	1.232	3.2
0.875 (0.875)	1.533 (1.526)	(9,8)	1.169	28.1
0.884 (0.887)	1.450 (1.433)	(11,6)	1.185	20.4
0.921 (0.924)	1.450 (1.436)	(12,4)	1.145	13.9
0.935 (0.937)	1.566 (1.555)	(9,7)	1.103	25.9

[a] Two last columns indicate the diameter, *d*, and chiral angle, α, of the assigned nanotubes. [b] These values fall in the gap between the laser excitation energies applied in this work and are approximate. The other PL emission and excitation energies were determined with the accuracy better than ±0.5%.

and emitters in the SWNT dispersion. A much higher quantum yield is expected for specific nanotubes contributing to the strongest bands in the PL spectra.

3.3. Structural Assignment of Nanotubes from the Photoluminescence Data. The solvent relaxation shifts of PL appear to be very small in dispersed SWNTs;[7] therefore, their emission−excitation maxima correspond accurately to the E_{11}^S and E_{22}^S transition energies and can be attributed to specific (*n*,*m*) nanotubes. The energies of the well-defined PL maxima of dispersed SWNTs observed in this work are listed in Table 1. These values could be most accurately determined using the two-dimensional contour plot of the PL intensity versus emission and excitation wavelengths (Supporting Information).

In the above discussion, we have frequently made use of the tight-binding model to qualitatively describe characteristic features of the optical absorption and luminescence of SWNTs. However, this model is apparently not accurate enough for the assignment of PL energies to specific semiconducting nanotubes, i.e., with specific (*n*,*m*) indices, as illustrated in Figure 6a. It has been mentioned above that this model predicts, reasonably well, an energy scale of E_{22}^S, E_{33}^S, and E_{11}^M branches (Figure 1) in the absorption and PL spectra. However, the emission (and S1 absorption) energies are, on average, ∼1.2 times larger than those predicted by the tight-binding model. Therefore, the E_{11}^S and E_{22}^S points from the PL spectra are right-shifted in Figure 6a relative to the calculated ones. The shift may be explained by taking into account Coulomb interaction among electrons.[25,26] According to the calculation of Ando,[25] the S1 band in fact represents the absorption of the lowest excitonic state in semiconducting nanotubes and is energy upshifted. In contrast, the S2 and S3 bands remain almost unperturbed. The NIR luminescence of SWNTs is then also of excitonic origin. Moreover, the excitonic effects may depend on the specific (*n*,*m*) structure of SWNTs (not taken into account in the calculation of Ando). This would mean that the simple model dependence $E_{11}^S \sim 1/d$ (Figure 1) does not hold true. This could also probably explain a significantly wider degree of scatter of the measured E_{22}^S energies than that predicted by the tight-binding model, even after taking into account the effect of trigonal warping[17] on the energy dispersion relations (Figure 6a). We conclude that the (*n*,*m*) assignment of emitting nanotubes is not possible on the pure basis of the tight-binding model.

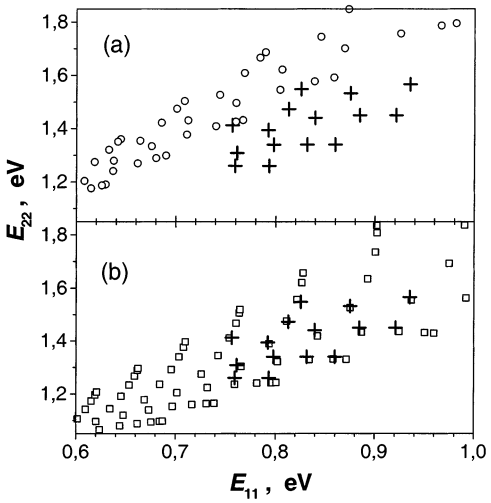

Figure 6. A comparison of the luminescence emission (E_{11})−excitation (E_{22}) maxima (crosses) with E_{11}^S and E_{22}^S energies calculated for semiconducting nanotubes in the E_{11}^S range of 0.6−1.0 eV using (a) the tight-binding model (cicles, calculated with $\gamma_0 = 2.9$ eV) and (b) the empirical relations (squares) derived by Bachilo et al. from the luminescence and Raman data for the HiPco nanotubes (ref 11).

Taking advantage of many well-resolved maxima in the PL spectra of the HiPco nanotubes, Bachilo et al. have very recently succeeded in an empirical modification of the tight-binding model E_{11}^S, $E_{22}^S - d$ relations to reproduce the PL maxima and to achieve their consistent (*n*,*m*) assignment.[11] We have found that these empirical relations describe our PL data as well (Table 1). A comparison between the PL maxima and the values calculated for all semiconducting nanotubes in the E_{11}^S range of 0.6−1.0 eV is also shown in Figure 6b. It is seen that all observed PL maxima can be unambiguously attributed to specific pairs of calculated E_{11}^S and E_{22}^S energies and, consequently, to specific (*n*,*m*) nanotubes. Table 1 shows the index assignment of the PL maxima following the procedure of Bachilo et al. According to this assignment, the majority of dispersed/emitting semiconducting nanotubes have a relatively large chiral angle, $15° \leq \alpha < 30°$. Only two tubes (16,2) and (15,1) with chiral angles smaller than 10°, and—similar to the HiPco nanotubes[11]—no (*n*,0) "zigzag" nanotubes with $\alpha = 0°$ were found. This suggests a relative stability and abundance of semiconducting nanotubes that have a large chiral angle. A more detailed analysis of the (*n*,*m*) distribution of nanotubes from their PL spectra depends on their relative absorption cross sections and PL quantum yields, which are not known yet. We conclude that the empirical relations of Bachilo et al. provide a consistent description of the photoluminescence data and accurate values of E_{11}^S and E_{22}^S energies of SWNTs in a broad diameter range. However, the physics behind these relations remains to be understood.

3.4. Luminescence Anisotropy. The structural anisotropy of carbon nanotubes (a high length/diameter ratio) suggests that their luminescence is polarized. Thus, Sun et al. observed significant luminescence anisotropy of functionalized SWNTs in solution and in polymeric matrixes.[5] This visible PL is likely caused by defects/chemical groups attached to nanotubes, with the latter serving as a polymeric backbone, thus rendering anisotropy to the emitters. Strong polarization effects have also been observed in resonant Raman spectra of SWNTs,[22] in particular, of isolated nanotubes grown on a substrate.[27]

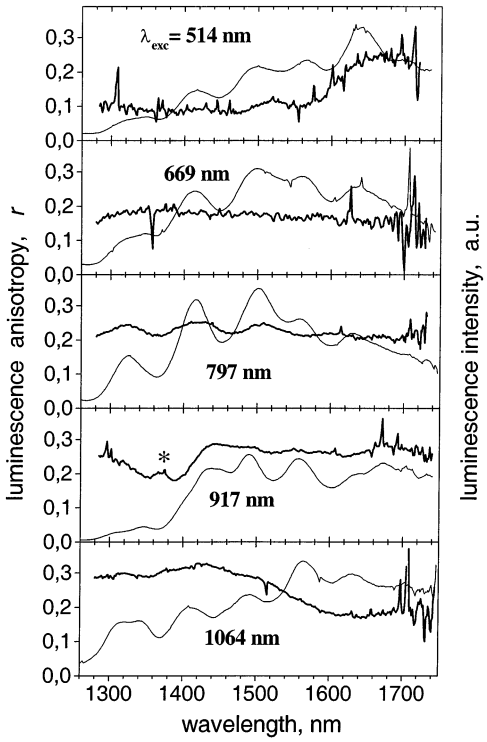

Figure 7. Luminescence anisotropy spectra (left axis, thick solid lines) relative to the luminescence intensity (right axis, thin solid lines) of SWNTs dispersed in D_2O/Tween-80 at selected laser excitation wavelengths. The asterisk on the 917 nm curve marks an artifact contribution due to a luminescence band of the Ti−sapphire laser.

We found that the NIR luminescence of dispersed SWNTs excited between 457 and 1064 nm is polarized with the positive anisotropy value r ranging from ∼0.1 up to 0.32 (Figure 7). For a single emitter, this would correspond to the emission dipole moment being displaced by 45° and 20°, respectively, from the absorption dipole moment ($r = 0.4$ for the collinear arrangement).[16] However, the luminescence anisotropy spectra shown in Figure 7 represent the averaged anisotropies of many emitting semiconducting nanotubes, with each having different electronic properties. Therefore, these spectra are quite complex, depending, like the luminescence intensity itself, on both the excitation and emission wavelengths.

The luminescence anisotropy of dispersed PLV nanotubes demonstrates the following characteristic features: (1) The value of r is, in general, low (∼0.1−0.15) for *S*3 absorption band excitation (Ar-ion laser lines). Many features in the anisotropy spectra do not follow those in the PL spectra. (2) Similar to the luminescence, the anisotropy does not depend on the excitation wavelength if this falls into the M1 band region (between 623 and 737 nm in our experiments); furthermore, it is practically invariant ($r \sim 0.18$) across the emission spectra upon excitation in this range. (3) When the S2 band region is excited (from about 750 up to ∼900 nm), the anisotropy is higher ($r \sim 0.2$−0.28) and its variation clearly correlates with the emission bands. (4) The highest values of r are observed at the longest excitation wavelengths (∼900−1064 nm). The corresponding anisotropy spectra correlate poorly with the PL features.

This complicated behavior can be understood, at least partially, as a consequence of the absorption anisotropy of semiconducting tubes that have two components, $A_{||}$ and $A_{\perp}$, for light polarized along, and normal to, the tube axis. According to the tight-binding model calculation of Lin,[24] the absorption spectra of SWNTs are dominated by $A_{||}$, which gives rise to the S1−S3 bands. According to the selection rules, $A_{\perp}$ corresponds to electronic transitions between other pairs of π/π^*-subbands. This absorption manifests an onset band between S1 and S2 and is almost featureless to shorter wavelengths.

The NIR luminescence of semiconducting nanotubes is due to the reverse of S1 optical excitation with the corresponding allowed emission polarized along the nanotube axis. Under the assumption that electronic relaxation in semiconducting tubes proceeds first to the lowest π^*-subband (nonradiatively) and then radiatively to the ground state, any excitation wavelength-dependent variations in PL anisotropy will be determined by the ratio of $A_{||}/(A_{\perp} + A_{||})$ which depends on the nanotube structure (n,m). This can explain the invariance of the anisotropy spectra excited in the M1 region, i.e., between the S2 and S3 bands ($A_{||}/A_{\perp} \sim$ constant for all semiconducting tubes) and correlations between the luminescence intensity and anisotropy upon excitation into the S2 band (Figure 7, $\lambda_{exc} = 797$ nm). The largest value of r is expected for excitation into the S1 band ($A_{\perp} = 0$).

The above anisotropy model is based on a substantial contribution of $A_{\perp}$ to the calculated absorption spectra of nanotubes. However, the measured spectra do not reveal any resolvable $A_{\perp}$ features (between the S1 and S2 bands). Furthermore, resonant Raman studies show that the absorption dipole moment (S2−S3 bands) is highly oriented along the nanotube axes.[22,27] Another complication could be the excitonic effects[25,26] already alluded to. These appear to be important for the S1 absorption as well as for the luminescence. Their influence on the luminescence anisotropy and possible dependence on nanotube chirality are not known yet. Finally, the anisotropy could also be affected by curvature of the quite flexible[9] and long[28] SWNTs in dispersion. If electronic excitation can propagate along the tube, but the emission arises from a relatively localized (e.g., due to the tube bending) electronic configuration, the anisotropy will be reduced because of multiple local orientations of the tube. A clarification of these issues requires polarized luminescence studies on aligned and isolated nanotubes.

Depolarization via molecular motions was evoked for the visible PL of functionalized SWNTs in a nonviscous solution at room temperature.[5] Decay of such PL can be quite slow, occurring over a time scale of nanoseconds,[4] i.e., comparable to the time scale of rotational diffusion of flexible polymers.[16] However, here we can rule out rotational diffusion of dispersed SWNTs as a possible reason for the luminescence anisotropy reduced with regard to the maximal value $r = 0.4$. Electronic relaxation in as-prepared solid SWNT samples is extremely fast and occurs within tens of femtoseconds.[29] The characteristic time of electronic relaxation in dispersed individual tubes or small bundles of weakly interacting tubes is not known yet. However, the complex variation of the anisotropy by changing the excitation and emission wavelengths (Figure 7) suggests that relaxation is still so fast that the nanotubes are "frozen" on the luminescence time scale. This would also be consistent with the low quantum efficiency of PL.

As was mentioned in the Experimental Section, dispersions of PLV nanotubes also showed a weak, structureless background photoluminescence below ∼1000 nm, in particular, under excitation with Ar-ion laser lines. This PL was found to be depolarized ($r = 0$), supporting the suggestion that it may be due to fullerenes and other organic impurities in the raw SWNT material. Prolonged sonication of SWNT dispersions in air resulted in an increase of the background PL, in particular, below ∼800 nm. The appearance of polarization ($r \sim 0.05$−0.1 at 650

nm) suggests another origin of the additional luminescence, probably caused by sonochemical oxidation of nanotubes.

3.5. Other SWNT Materials. For comparison with the PLV carbon nanotubes, we measured a photoluminescence of dispersions of other SWNT materials. One of the samples was the raw SWNTs obtained by electric arc vaporization (EAV) of carbon loaded with Ni/Y catalysts.[30] These nanotubes have a typical diameter distribution between about 1.2 and 1.6 nm, which depends on the catalyst composition and process parameters.[31] A D_2O/Tween-80 dispersion of the EAV nanotubes that we tested also demonstrated NIR luminescence; however, it was mainly at wavelengths beyond the sensitivity range of our detector. According to the PL spectra, this material contained practically no (dispersed) nanotubes with diameters smaller than ~1.3 nm.

An oxidative treatment, typically with boiling nitric acid, is often applied to raw SWNTs to purify them by removing metal catalysts and amorphous carbon as well as to modify them chemically.[9] However, the introduced structural defects and chemical (carboxyl) groups are expected to strongly affect the electronic properties of SWNTs. We found that such oxidative treatment of the PLV nanotubes (8 h reflux in 3 M HNO_3, then thoroughly washed and dispersed in D_2O/Tween-80) had a dramatic effect on their NIR luminescence. Compared to as-prepared SWNTs, a dispersion of the acid-treated SWNTs showed a much weaker and poorly structured PL, which was red shifted and only moderately dependent on the excitation wavelength. The red shift of PL may be due to changes in the electronic structure of the treated SWNTs, preferential oxidation of SWNTs with smaller diameters,[9] or, most likely, both reasons. Furthermore, the acid-treated SWNTs showed a significantly stronger background PL below ~1200 nm with the intensity increasing smoothly toward the excitation wavelength. In fact, a yellowish component of this PL excited by an Ar-ion laser line could be seen by the naked eye. The emitters of this PL are likely related to structural defects on the acid-treated nanotubes.

It has been shown that SWNTs form relatively stable (with lifetimes of a few days) suspensions under sonication in *N*,*N*-dimethylformamide (DMF) and that very thin bundles or possibly individual nanotubes can be loaded onto an amine-coated silicon wafer[32] or selectively deposited onto electrode circuites[33] from such dilute suspensions. This suggests that individual tubes/small bundles can be stabilized in DMF, at least for a short time after sonication. However, we have detected practically no NIR luminescence from fresh dispersions of the as-prepared and acid-treated PLV nanotubes in this solvent. The luminescence appears to be quenched because of the relatively strong interactions of SWNTs with DMF molecules, presumably of a charge-transfer character.

4. Concluding Remarks

We have found that SWNTs prepared by the laser vaporization method and ultrasonically dispersed in a D_2O−surfactant mixture show near-infrared PL, corresponding to the lowest electronic interband transtions (E_{11}^S) of semiconducting nanotubes, analogous to the PL reported recently for the HiPco nanotubes that have smaller diameters by O'Connell et al.[7] Thus, such luminescence appears to be a common property of SWNTs. Remarkable features of this PL are multiple emission bands with a strong resonance-like dependence on the excitation wavelength and complex polarization anisotropy, depending on both the excitation and emission wavelengths.

Such luminescence is likely to become a valuable tool for characterization of SWNTs, because it is selective to semiconducting tubes and directly provides the energies of the lowest interband transitions E_{11}^S (from emission bands) and E_{22}^S (from resonances in the excitation spectra). In comparison to the absorption spectra, PL appears to be much more sensitive to the changes of the electronic structure of SWNTs, caused, for instance, by chemical treatment. On the other hand, our results suggest that the quantum efficiency of PL decreases with the increasing nanotube diameter; therefore, its observation is probably limited to nanotubes with diameters up to ~1.5 nm (at present technology).

The luminescence features agree only qualitatively with the simple tight-binding model of the electronic structure of SWNTs.[9] On the other hand, all observed PL maxima could be satisfactorily correlated with the E_{11}^S and E_{22}^S values and specific (n,m) indices using the empirical relations derived recently by Bachilo et al. for the HiPco nanotubes.[11] According to this assignment, mostly the large chiral angle ($15° \leq \alpha < 30°$) and no zigzag ($\alpha = 0°$) semiconducting nanotubes contribute to the luminescence of SWNTs prepared by the laser vaporization method.

According to the inference of O'Connell et al.,[7] the NIR luminescence is mainly due to individual nanotubes isolated from each other in surfactant micelles. Indeed, the luminescence is almost totally quenched in solid SWNT samples, and ultrasonic dispersion of SWNT bundles in a water−surfactant mixture seems to be a critical step in observing the intrinsic NIR luminescence of nanotubes. However, we cannot rule out the possibility of luminescence from small bundles with relatively weakly interacting nanotubes and of energy transfer between (semiconducting) nanotubes. To examine the role of intertube interactions at this limit, experiments on well-defined systems of isolated bundles or aligned individual nanotubes are necessary. The extraordinary photostability of SWNTs under intense laser irradiation and relatively efficient PL, at least for SWNTs with diameters around 1 nm,[7] make such experiments promising.

Finally, we remark that dispersed micelle-isolated nanotubes are also a very interesting object for resonant Raman studies, ultimately of single nanotubes. According to our first results, the dispersed nanotubes show significantly sharper and modified Raman features with regard to the solid material.

Acknowledgment. The support of this work by the Deutsche Forschungsgemeinschaft under SFB 551 and by BMBF is gratefully acknowledged. The authors thank C. Journet for a sample of carbon nanotubes prepared by the arc vaporization method and R. B. Weisman for sending a preprint (ref 11) prior to publication.

Supporting Information Available: Near-infrared luminescence spectra of a SWNT dispersion in a D_2O/Tween-80 at 35 different excitation laser wavelengths from 457 up to 1064 nm presented as separate curves as well as in the form of a two-dimensional contour plot (luminescence intensity versus emission and excitation wavelengths). This material is available free of charge via the Internet at http://pubs.acs.org.

References and Notes

(1) Kataura, H.; Kumazawa, Y.; Maniwa, Y.; Umezu, I.; Suzuki, S.; Ohtsuka, Y.; Achiba, Y. *Synth. Met.* **1999**, *103*, 2555.

(2) Jost, O.; Gorbunov, A. A.; Pompe, W.; Pichler, T.; Friedlein, R.; Knupfer, M.; Reibold, M.; Bauer, H.-D.; Dunsch, L.; Golden, M. S.; Fink, J. *Appl. Phys. Lett.* **1999**, *75*, 2217.

(3) Vivien, L.; Anglaret, E.; Riehl, D.; Bacou, F.; Journet, C.; Goze, C.; Andrieux, M.; Brunet, M.; Lafonta, F.; Bernier, P.; Hache, F. *Chem. Phys. Lett.* **1999**, *307*, 317. Chen, P.; Wu, X.; Sun, X.; Lin, J.; Ji, W.; Tan,

K. L. *Phys. Rev. Lett*. **1999**, *82*, 2548. Riggs, J. E.; Walker, D. B.; Caroll, D. L.; Sun, Y.-P. *J. Phys. Chem*. **2000**, *B104*, 7071.

(4) Riggs, J. E.; Guo, Z.; Carroll, D. L.; Sun, Y.-P. *J. Am. Chem. Soc*. **2000**, *122*, 5879.

(5) Sun, Y.-P.; Zhou, B.; Henbest, K.; Fu, K.; Huang, W.; Lin, Y.; Taylor, S.; Carroll, D. L.; *Chem. Phys. Lett.* **2002**, *351*, 349.

(6) Nagasawa, N.; Sugiyama, H.; Naka, N.; Kudryashov, I.; Watanabe, M.; Hayashi, T.; Božović, I.; Božović, N.; Li, G.; Li, Z.; Tang, Z. K. *J. Lumin*. **2002**, *97*, 161.

(7) O'Connell, M. J.; Bachilo, S. M.; Huffman, C. B.; Moore, V. C.; Strano, M. S.; Haroz, E. H.; Rialon, K. L.; Boul, P. J.; Noon, W. H.; Kittrell, C.; Ma, J.; Hauge, R. H.; Weisman, R. B.; Smalley, R. E. *Science* **2002**, *297*, 593.

(8) Bronikowski, M. J.; Willis, P. A.; Colbert, D. T.; Smith, K. A.; Smalley, R. E. *J. Vac. Sci. Technol.* **2001**, *A19*, 1800.

(9) Saito, R.; Dresselhaus, G.; Dresselhaus, M. S. In *Physical Properties of Carbon Nanotubes*; Imperial College Press: London, 1998.

(10) Guo, T.; Nikolaev, P.; Thess, A.; Colbert, D. T.; Smalley, R. E. *Chem. Phys. Lett*. **1995**, *243*, 49. Rinzler, A. G.; Liu, J.; Dai, H.; Nikolaev, P.; Huffman, C. B.; Rodriguez-Macias, F. J.; Boul, P. J.; Lu, A. H.; Heymann, D.; Colbert, D. T.; Lee, R. S.; Fisher, J. E.; Rao, A. M.; Eklund, P. C.; Smalley, R. E. *Appl. Phys.* **1998**, *A67*, 29.

(11) Bachilo, S. M.; Strano, M. S.; Kittrell, C.; Hauge, R. H.; Smalley, R. E.; Weisman, R. B. *Science* **2002**, *298*, 2361.

(12) Lebedkin, S.; Schweiss, P.; Renker, B.; Malik, S.; Hennrich, F.; Neumaier, M.; Stoermer, C.; Kappes, M. M. *Carbon* **2002**, *40*, 417.

(13) Hennrich, F.; Lebedkin, S.; Malik, S.; Tracy, J.; Barczewski, M.; Rösner, H.; Kappes, M. M. *Phys. Chem. Chem. Phys*. **2002**, *4*, 2273.

(14) Shimizu, O.; Watanabe, J.; Imakubo, K.; Naito, S. *Chem. Lett*. **1999**, 67.

(15) Arbogast, J. W.; Foote, C. S. *J. Am. Chem. Soc*. **1991**, *113*, 8886.

(16) Lakowicz, R. J. In *Principles of Fluorescence Spectroscopy*, 2nd ed.; Kluwer Academic/Plenum Publisher: New York, 1999; Chapter 10.

(17) Saito, R.; Dresselhaus, G.; Dresselhaus, M. S. *Phys. Rev*. **2000**, *B61*, 2981.

(18) Reich, S.; Thomsen, C.; Ordejón, P. *Phys. Rev*. **2002**, *B65*, 155411.

(19) Pichler, T.; Knupfer, M.; Golden, M. S.; Fink, J.; Rinzler, A.; Smalley, R. E. *Phys. Rev. Lett*. **1998**, *80*, 4729.

(20) Absorption of the SWNT film measured in a Spectralon integrating sphere (Labsphere) shows the same features as the spectrum in Figure 2, but with a lower background. The difference is due to light scattering and becomes particularly significant (>30% of the background) below ~500 nm (unpublished results). Light scattering in the centrifuged SWNT dispersion is not significant; therefore, Figure 2b represents practically its true optical absorption.

(21) Chen, J.; Hamon, M. A.; Hu, H.; Chen, Y.; Rao, A. M.; Eklund, P. C.; Haddon, R. C. *Science* **1998**, *282*, 95.

(22) Dresselhaus, M. S.; Eklund, P. C. *Adv. Phys*. **2000**, *49*, 705 and references therein.

(23) Strictly speaking, these (polarized) luminescence spectra measured without an emission polarizer but with polarized laser excitation do not represent the total luminescence intensity $I_T(\lambda) = I_{VV}(\lambda) + 2I_{VH}(\lambda)$ (ref 16). However, they deviate only slightly from I_T (λ), because of the predominance of the I_{VH} component and relatively small variation of the luminescence anisotropy across the spectra (Figure 7), i.e., spectral similarity of the I_{VV} and I_{VH} components.

(24) Lin, M. F. *Phys. Rev*. **2000**, *B62*, 13153.

(25) Ando, T. *J. Phys. Soc. Jpn*. **1997**, *66*, 1066.

(26) Ichida, M.; Mizuno, S.; Tani, Y.; Saito, Y.; Nakamura, A. *J. Phys. Soc. Jpn*. **1999**, *68*, 3131.

(27) Jorio, A.; Souza Filho, A. G.; Brar, V. W.; Swan, A. K.; Ünlü, M. S.; Goldberg, B. B.; Righi, A.; Hafner, J. H.; Lieber, C. M.; Saito, R.; Dresselhaus, G.; Dresselhaus, M. S. *Phys. Rev*. **2002**, *B65*, 121402.

(28) A typical length of a few hundred nanometers was estimated for SWNTs ultrasonically dispersed and deposited on a substrate (ref 32b, 33).

(29) Hertel, T.; Moos, G. *Chem. Phys. Lett*. **2000**, *320*, 359.

(30) Journet, C.; Maser, W. K.; Bernier, P.; Loiseau, A.; de la Chapelle, M. L.; Lefrant, S.; Deniard, P.; Lee, R.; Fischer, J. E. *Nature* **1997**, *388*, 756.

(31) Takizawa, M.; Bandow, S.; Yudasaka, M.; Ando, Y.; Shimoyama, H.; Iijima, S. *Chem. Phys. Lett*. **2000**, *326*, 351.

(32) (a) Liu, J.; Casavant, M. J.; Cox, M.; Walters, D. A.; Boul, P.; Lu, W.; Rimberg, A. J.; Smith, K. A.; Colbert, D. T.; Smalley, R. E. *Chem. Phys. Lett*. **1999**, *303*, 125. (b) Krupke, R.; Malik, S.; Weber, H. B.; Hampe, O.; Kappes, M. M.; Löhneysen, H. v. *Nano Lett*. **2002**, *2*, 1161.

(33) Krupke, R.; Hennrich, F.; Weber, H. B.; Beckmann, D.; Hampe, O.; Malik, S.; Kappes, M. M.; Löhneysen, H. v. *arXiv.org e-Print archive, Cond. Matt*. **2002**, 0201574.